Design of an optimized nested-mirror neutron reflector for a NNBAR experiment

Citation for the original published paper (version of record):
Wagner, R., Barrow, J., Bohm, C. et al (2023). Design of an optimized nested-mirror neutron reflector for a NNBAR experiment. Nuclear Instruments and Methods in Physics Research, Section A: Accelerators, Spectrometers, Detectors and Associated Equipment, 1051. http://dx.doi.org/10.1016/j.nima.2023.168235

Nuclear Inst. and Methods in Physics Research, A 1051 (2023) 168235

Contents lists available at ScienceDirect

Nuclear Inst. and Methods in Physics Research, A

journal homepage: www.elsevier.com/locate/nima

Full Length Article

Design of an optimized nested-mirror neutron reflector for a NNBAR experiment

R. Wagner [a,*], J. Barrow [b,c], C. Bohm [d], G. Brooijmans [e], H. Calen [f], J. Cederkäll [g], J. Collin [h], K. Dunne [d], L. Eklund [f], P. Fierlinger [i], U. Friman-Gayer [j], M. Frost [k], M. Holl [j], T. Johansson [f], Y. Kamyshkov [l], E. Klinkby [m], A. Kupsc [f], B. Meirose [d,g], D. Milstead [d], A. Nepomuceno [n], T. Nilsson [o], A. Oskarsson [g], H. Perrey [g], B. Rataj [j], N. Rizzi [m], V. Santoro [j,g], S. Silverstein [d], A. Takibayev [j], M. Wolke [f], S.C. Yiu [d], A.R. Young [p], L. Zanini [j], O. Zimmer [a]

[a] Institut Laue-Langevin, 71 Avenue des Martyrs, 38042 Grenoble, France
[b] Massachusetts Institute of Technology, Department of Physics, Cambridge, MA 02139, USA
[c] School of Physics and Astronomy, Tel Aviv University, Tel Aviv 69978, Israel
[d] Department of Physics, Stockholm University, 106 91 Stockholm, Sweden
[e] Department of Physics, Columbia University, New York, NY 10027, United States of America
[f] Department of Physics and Astronomy, Uppsala University, Uppsala, Sweden
[g] Department of Physics, Lund University, P.O. Box 118, SE-221 00 Lund, Sweden
[h] Department X, Télécom Physique Strasbourg, 300 Bd Sébastien Brant, 67412 Illkirch, France
[i] Physikdepartment Technische Universität München James-Franck-Str. 1, 85748, Garching, Germany
[j] European Spallation Source ERIC, Partikelgatan 5, 22484 Lund, Sweden
[k] Neutron Technologies Division, Oak Ridge National Laboratory, Oak Ridge, TN 37831, USA
[l] Department of Physics and Astronomy, The University of Tennessee, Knoxville, TN 37996, USA
[m] DTU Physics, Technical University of Denmark, Frederiksborgvej 399, DK-4000 Roskilde, Denmark
[n] Departamento de Ciências da Natureza, Universidade Federal Fluminense, Rua Recife, 28890-000 Rio das Ostras, RJ, Brazil
[o] Institutionen för Fysik, Chalmers Tekniska Högskola, Sweden
[p] Department of Physics, North Carolina State University, Raleigh, NC 27695-8202, USA

ARTICLE INFO

Keywords:
Instrumentation for neutron sources
Neutron optics
Monte-Carlo simulations

ABSTRACT

The NNBAR experiment for the European Spallation Source will search for free neutrons converting to antineutrons with an expected sensitivity improvement of three orders of magnitude compared to the last such search. This paper describes both the simulations of a key component for the experiment, the neutron optical reflector and the expected gains in sensitivity.

1. Introduction

The Standard Model (SM) of particle physics has undergone numerous high precision tests and is yet to be falsified outside of the neutrino sector. However, it does not address a number of major open questions in modern physics and physics beyond the SM is thus expected.

A topical open issue is the origin via a baryogenesis mechanism of the observed asymmetric abundances of matter and antimatter in our known universe. Sakharov pointed out that any baryogenesis process must include Baryon Number Violation (BNV) [1]. A possible candidate process of BNV is the transformation of a neutron to an antineutron [2]. Such a process violates baryon number (B) by $|\Delta B| = 2$ and, when using free neutrons, is a clean channel with which to look for BNV. The process is featured in dedicated models of baryogenesis [3–5] and other theories beyond the SM such as supersymmetry [6,7] and extra dimensions [8,9]. The neutron transformation may occur while free neutrons are propagating to a detector, where the antineutron will annihilate in a target and be detected via the multi-pion production signature. The last search with free neutrons was done in the early 1990's at the ILL and set the current lower limit for free neutron–antineutron oscillation time: $\tau > 0.86 \times 10^8$ s [10]. Experiments with free neutrons are not the only option to search for neutron to antineutron oscillations. We would like to mention that one proposes to utilize ultra cold neutrons (UCN) stored in a bottle [11] and another one that suggests the use of a special guide for reflecting the antineutron part of the wave function [12]. A yet new search experiment with free neutrons, NNBAR [13], has been proposed for the European Spallation Source (ESS) [14] in Lund. NNBAR aims at an improvement in sensitivity of three orders of magnitude compared

* Corresponding author.
E-mail address: wagnerrichard@ill.fr (R. Wagner).

https://doi.org/10.1016/j.nima.2023.168235
Received 30 September 2022; Received in revised form 16 March 2023; Accepted 21 March 2023
Available online 23 March 2023
0168-9002/

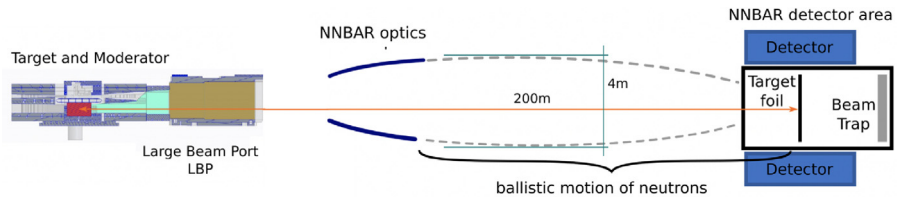

Fig. 1. Schematic overview of the NNBAR experiment (not in scale) with a focus on the reflector configuration used in the Monte-Carlo simulations. The moderator (source) to detector distance is 200 m. The transversal dimension of the reflector is bounded by diameter of 4 m. The annihilation target is of radius 1 m. Vacuum tube and magnetic shielding are not shown.

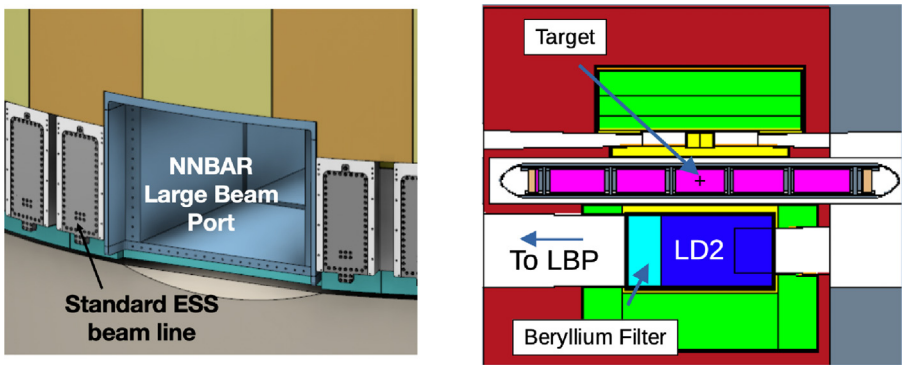

Fig. 2. (left) Side by side schematic of standard ESS beam line extraction ports and the LBP that is about three times the size of the former. (right). Schematic of the liquid deuterium moderator.

to the ILL search. The ESS, currently under construction, is designed to be the most powerful neutron source in the world. The HighNESS program [15,16] comprises the design of a liquid deuterium (LD) moderator that would be used as a cold high-flux source for NNBAR. HighNESS allows also the design of all components of the experiment to be developed — neutron source, the neutron focusing and transport and the NNBAR detector [17]. For this paper one particular aspect of such a NNBAR experiment, namely the design of a neutron focusing and transport system, has been studied. Details on other important areas such as e.g. the detector and the moderator can be found in the recently published overview article [18].

2. The NNBAR experiment

In Fig. 1a schematic diagram of the set-up of the planned NNBAR experiment at the ESS is shown. Neutrons that are generated at the spallation target are slowed in a moderator and traverse out of the large beam port (LBP). The LBP is a special neutron extraction port that covers three regular beam ports (see Fig. 2) and has been designed specifically for the NNBAR experiment (see Section 2 of Ref. [18]). To make use of the large solid angle accessible throughout the LBP, a system of elliptical shaped neutron guides is placed in the region behind the LBP's exit to focus the neutrons in the direction of the detector located upstream. After having passed the optics, neutrons fly in a magnetically shielded region to the detector region at the end of the beam-line. The moderator (source) to detector distance is foreseen to be 200 m. To reach the goal of a performance increase of three orders of magnitude compared to the previous experiment, the optimization of the whole NNBAR experiment is currently on-going [18]. This paper describes the optimization of the neutron optics system that will transport the neutron to the experimental area where a detector able to reveal the signature of an antineutron annihilation will be located. The detector system, comprising calorimetry and tracking is being designed to observe the multi-pion final state arising from the annihilation of the antineutron at the target foil [19].

The LD2 moderator. The main source of the NNBAR experiment will be a cold moderator, to be placed below the spallation target, at the location of maximum flux that will allow to reach a source of maximum intensity. The material for this source is liquid deuterium at about 20 K temperature and the size of the moderator will be distinctively larger, compared to the upper moderator of the ESS (See Section 3 of Ref. [18]). It will deliver a high neutron intensity rather than a high brightness. The expected peak heat load on the moderator is of around $Q = 57\,\mathrm{kW}$. The cryogenic system of the moderator is technically designed to cope with these loads [15]. The moderator is box-shaped, with a large (24 cm high, 40 cm wide) opening on the side directed to the NNBAR experiment (see Fig. 2). The length of the moderator is 48 cm. In the extraction window a large cold beryllium (Be) filter block of depth 13 cm is placed to increase the flux above 4 Å. The size of the moderator and the extraction window including the filter have been optimized to provide the best high intensity flux for the sensitivity of the NNBAR experiment. As an optimization parameter for the moderator design λ^2 was chosen to take into account that lower wavelengths (i.e. longer flight times) contribute more to the figure of merit (FOM) of a NNBAR experiment (for the definition see section below).

3. The NNBAR focusing reflector

In order for NNBAR to exploit the neutron flux from LBP, a reflector is needed to ensure that a large amount of the flux passing the LBP aperture is directed and focused through the magnetically shielded region onto the annihilation target. The large-aperture neutron reflector plays a major role in the increase of sensitivity of the search. The probability of a free $n \to \bar{n}$ transformation is given by $P_{n\to\bar{n}} = \langle t^2\rangle/\tau_{osc}^2$, where $\langle t^2\rangle$ is an average square of the free flight time of neutrons in the experiment and τ_{osc} is the characteristic time of $n \to \bar{n}$ transformation for free neutrons in a vacuum. The present limit on τ_{osc} was set three decades ago in the previously mentioned state-of-the-art experiment made with a cold neutron beam at the ILL reactor ($\tau_{osc} \geq 0.86 \times 10^8$ s) [10]. The figure of merit (FOM) for a free $n \to \bar{n}$ search is given by FOM $= N \cdot \langle t^2\rangle$, where N is the number of free neutrons arriving after an average time-squared, $\langle t^2\rangle$, on the detector target. In our simulations

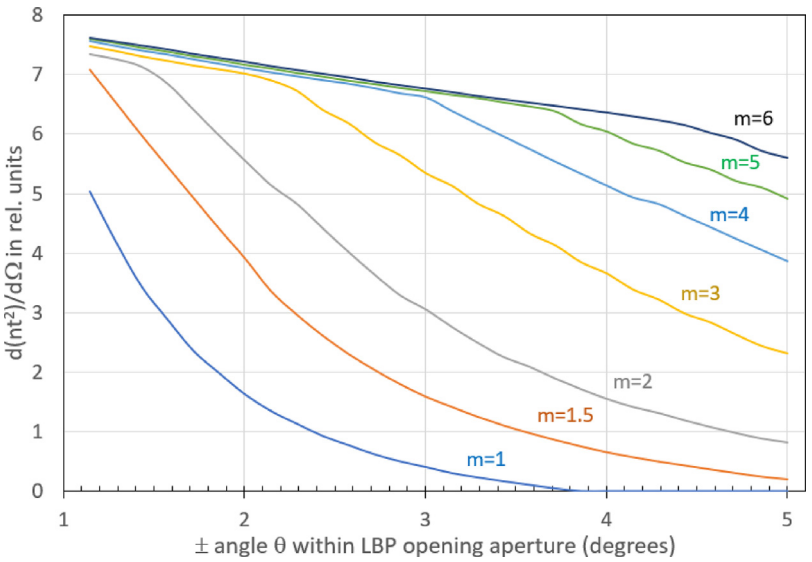

Fig. 3. The sensitivity $N\langle t^2\rangle$ that can be provided by the $d\Omega$ element of the super-mirror reflector with different m-values as a function of the θ location of $d\Omega$ within the LBP opening aperture. For a maximum LBP opening $\pm 5°$, $m = 6$ reflection quality [20] is adequate for the NNBAR design goal. The total FOM figure should be obtained by integration between minimum and maximum θ angles covered by the actual reflectors.

we have the exact uninterrupted flight time t_i and the weight (intensity resp. neutrons/second) n_i of each neutron arriving at the detector. The FOM is then derived calculating $\sum_i n_i \cdot t_i^2$. To have a quantity that can be easily compared with previous searches, the FOM is normalized (as described in Ref. [13]) with the FOM of the above mentioned experiment at the ILL that ran for one year, so that the FOM is given as quantity of ILL units per year. A value of FOM = 1 corresponds to a sensitivity equal to that achieved at the ILL. All FOM values provided in this paper are expressed this way. For the sensitivity it is important to note the following. At a distance, L, from the cold source to the detector, with area, A, the fraction of neutrons collected by the detector will be proportional to the seen solid angle: $N \sim \Delta\Omega = A/L^2$. For neutrons with average velocity, v, the time-of-flight squared will be $\langle t^2\rangle = L^2/v^2$. It is therefore seen that the sensitivity does not depend directly on L and an increase is also possible by providing a high flux of slow neutrons with large $\langle t^2\rangle$.

With the above discussion of sensitivity in mind, the concept of the elliptical focusing reflector [21] can be used. Lambertian brightness emission from cold neutron moderator surface can be intercepted by a large open aperture and super-mirror reflector elements installed within this aperture. This directs neutrons to the annihilation target by a single reflection. An important performance parameter of super-mirror reflectors is the m-value [20]. Given an aperture opening of $\pm 4°$ degrees one can consider the small element of the mirror reflecting surface located within $d\Omega = d\cos\theta d\varphi$ inside the LBP opening at some distance z from the cold source and study the question of the quality of super-mirror reflecting material that is needed to provide the change of the neutron trajectory. This change allows neutrons from the source to reach the annihilation target. In Fig. 3 such a calculation for the baseline reflector (see Section 5.1 and Fig. 12) is depicted for the configuration in an idealized situation with a point-like cold source, z-axis symmetric reflection, and without taking effects caused due to gravity and off-specular reflection into account. As an example: a nested mirror layout, as described in the following section, that covers an aperture opening of $\pm 4°$ degrees has gains in terms of FOM for subsequently increased m-values as collected in Table 1. As expected for an m-values larger than 6 no further gain is achieved.

Table 1
Gains in FOM that can be achieved by increasing the m-value of a nested mirror reflector that covers an opening of $\pm 4°$. After $m > 6$ no significant gain is attained.

m-value	1	1.5	2	3	4	5	6	7	8
Relative gain	–	1.11	0.55	0.51	0.16	0.06	0.01	0.00	0.00
Absolute gain	–	1.11	2.29	3.97	4.74	5.09	5.17	5.23	5.23

3.1. Nested mirror optics

A possible architecture which transports neutrons diverging from a source to a detector is an elliptical guide. The surfaces of such a device have the shape of an ellipse where, the focal points coincide with the center of the source and the detector, respectively [22,23]. An ellipse has the optical property that a beam that emanates from one of its focal points is reflected directly to the other one. Since this feature does not apply to rays starting not at the focal points, the ellipse is therefore a non-imaging device. Nested layers of several guides are able to build up a spatial tight optical component. If the outer layer of such a nested elliptical guide is given, the inner layers can be designed in a recursive manner such that the layers will not shadow themselves. In the diagram shown in Fig. 4 the construction principle is shown. The finite size of the optical layers is currently not taken into account.

Different nested layouts of the reflector that are symmetrical around the z-axis are possible. These are (a) a mono planar, (b) a double planar, and (c) a cylindrical system. In Fig. 5 three dimensional diagrams of the different types are shown. In a double mono planar reflector, neutrons would have to be reflected twice in order to be directed to the center of the detector. For the cylindrical symmetrical case, only one reflection is needed. The mono planar reflector comprises two separated devices that are rotated by ninety degrees with respect to each other such that one component acts as a horizontal and the other as a vertical reflector. From an engineering perspective this configuration seems to be particularly promising.

A difficulty of the nested reflector design is the thickness of the glass substrate which is used for the construction of the stable high-quality industrial super-mirrors. Recent developments of self-sustaining substrate less super mirrors [24] offer an elegant possible solution to this problem.

3.2. Magnification of an elliptical reflector

For any portion of a perfect (without accounting for gravity effects) rotational ellipsoid surface, a point-like emission source in one focal point is projected exactly to the image point in the other focal point.

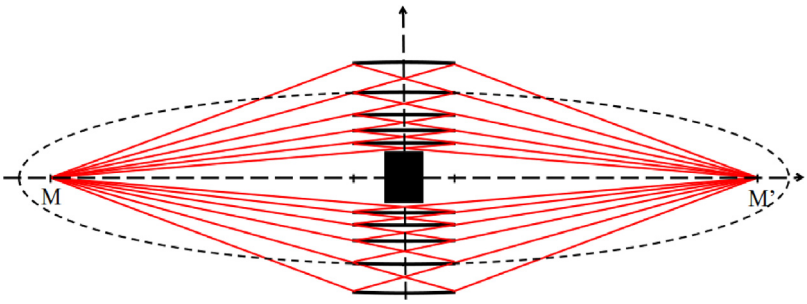

Fig. 4. Schematic of a nested elliptical guide. M and M' are common focal points of the ellipses forming the layers (the dashed line shows one of them).

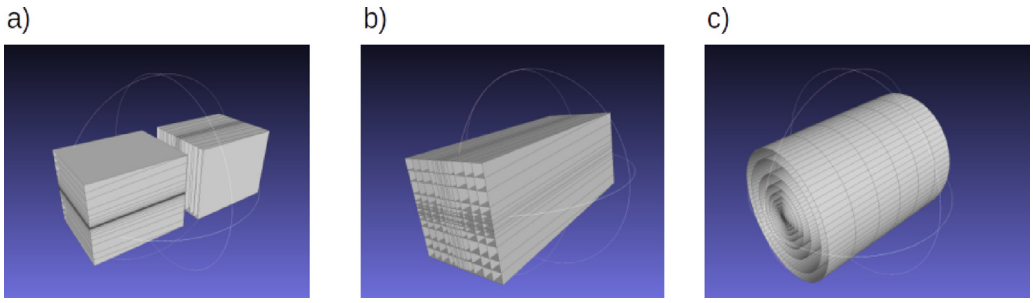

Fig. 5. Types of nested optical components (a) mono planar (b) double planar (c) cylindrical.

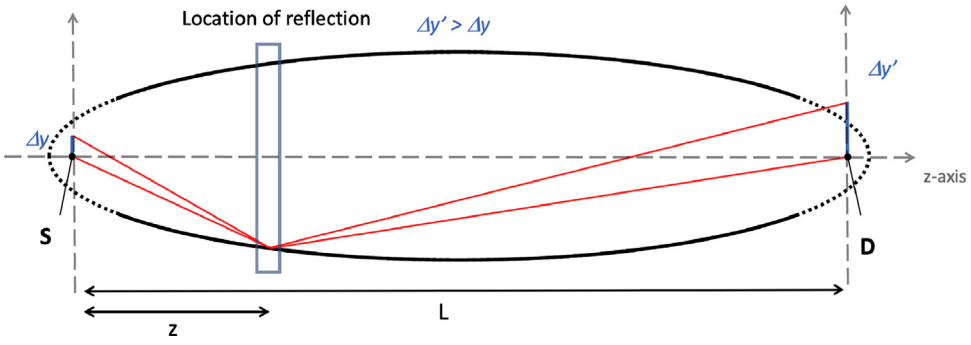

Fig. 6. Off-Axis magnification of an elliptical reflector. With origin at the Source S in the left focal point, L distance between focal Points and to the detector D, z coordinate of reflection along z-axis. $\Delta y'$ is the off axis height at the source and $\Delta y'$ is the height at the detector.

However, as is the case for any realistic optical system, if the source point is displaced from the ellipsoid focus lateral to the optical z-axis then the image point will similarly be laterally displaced with a magnification factor. Fig. 6 summarizes this situation. The magnification M for an off axis point of height Δy at left sided focal point is [25]:

$$\Delta y = \frac{L - z}{z} \Delta y' \tag{1}$$

$$M = \Delta y / \Delta y' = \frac{L - z}{z} \tag{2}$$

With the origin in left focal point, L the distance between focal points and z the coordinate of reflection along the z-axis. $\Delta y'$ is the height at right side focal point. If, therefore, the reflection point Z_{refl} is 10 m away from the source and the focal distance is $L = 200\,\text{m}$, the magnification factor will be ~ 20. For a detector of radius $r = 1\,\text{m}$ the most "efficient" emission area of the source will then fall within a radius $\sim \pm 5$ cm from the ellipsoid axis. This effect of magnification can be studied in simulations; an example is given in Fig. 7. The positioning of the reflector between source and detector has a general property such that the nearer the moderator, the larger the covered solid angle albeit with a deterioration of the focusing and vice versa. The optimum position with regards to the FOM is a trade between these two effects.

Since the size of the source plays an important role in the capability of the reflector to transport neutrons from it to the detector, the properties and parameters of the focusing reflector are simultaneously optimized with the design of the cold moderator in an iterative process.

4. Basic reflector setup and simulations

A dedicated simulation framework (described in detail here [26]), including the design of the moderator, the neutron transport system to the detector, the magnetic shielding for the field-free propagation region and lastly the design of the detector that allows to observe an annihilation signal, is part of the NNBAR program. In this paper the focus is only on the simulation part for the optical reflector.

The principal setup for the reflector that is under study has been already shown in Fig. 1. The optic is supposed to start at a minimum distance of 10 m from the moderator center and the detector is placed 200 m away from the center of the moderator. The flight time is measured from the point in time of the last interaction (reflection) with the optic. The transversal dimension of the reflector is bounded by a maximum assumed tube width and height of 4 m. Gravity is turned on for all simulations.

To compare different geometries as well as the exact placement of the reflector system, neutron ray-tracing simulations are performed using `McStas` [27]. In `McStas`, the components that constitute an instrument are described in a high-level language that is then compiled

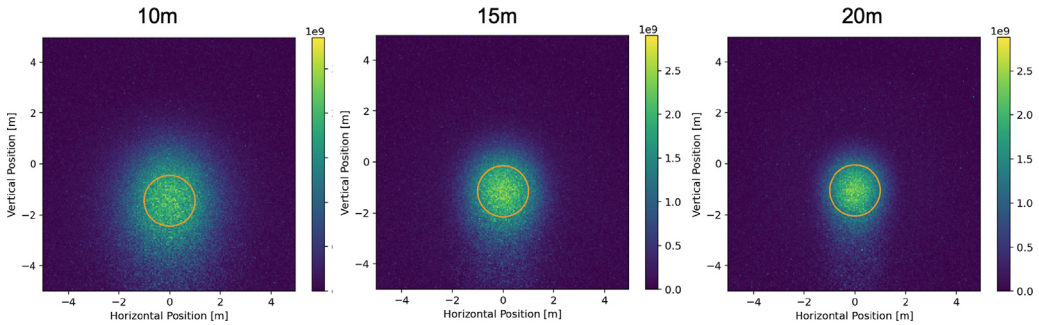

Fig. 7. Effect of magnification demonstrated for a 4-level nested elliptical reflector of 10 m length at varied starting positions. The neutrons arriving at 200 m weighed with their uninterrupted flight time squared are shown. The orange circle marks the supposed position of the actual antineutron detector of radius 1 m. The magnification gets less the later the reflector starts but the FOM is largest for the 15 m plot. It varies as trade off between focusing and covered solid angle.

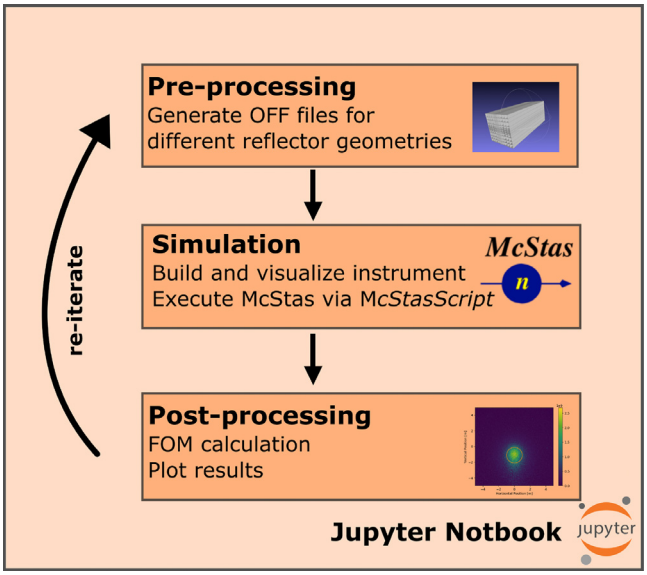

Fig. 8. Simulation strategy.

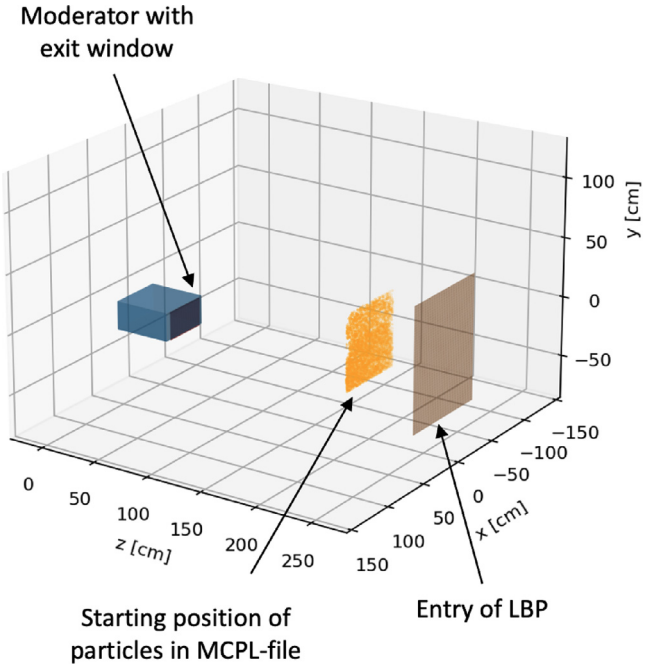

Fig. 9. MCPL source of the simulation. The particles are emitted from the moderator window, but already forward propagated to a distance of 2 m, just before the entry of the LBP.

into C–Code with which the Monte Carlo simulation is performed. An extension to `McStas` called `McStasScript`[1] allows one to control `McStas` via Python scripting (e.g. in JupyterLab[2] a web-based interactive python development environment). With `McStasScript` the whole simulation can reside and be performed in a common environment. The results can be readily accessed for post-processing such as FOM calculations and plotting operations. The source term is realized as an `MCPL_input` component [28]. It reads an MCPL-file [29], that contains a long list of neutrons that have been obtained as output from a dedicated MCNP [30] simulation of the moderator. In this input file the neutrons have been already propagated to an area located at 2 m from the center of the moderator (See Fig. 9). The divergence of the neutrons is already limited to the solid angle accepted by the LBP. This helps to increase the number of useful neutrons, reduces the time of the individual runs and provides a good particle statistics for the Monte-Carlo simulations. The geometry of the optics is described in the plain text, object file format (OFF-File). This file is generated automatically from a couple of input parameters by functions written in Python. The OFF-file is then used as input to the `McStas` component `Guide_anyshape`, to place and describe the reflector as well as the LBP is modeled as an OFF-File, too and utilizes again the `Guide_anyshape` component. Neutrons that hit the walls of the LBP are absorbed. A `Monitor_nD` component serves as detector where the velocity and flight time of the neutrons are recorded. This virtual detector of the simulation is of size 10 m × 10 m and hence distinctively larger then the real NNBAR detector. The output of this detector is a particle list with position, velocity, flight time and weight (neutrons/second). The FOM is calculated for the area of a circle with 1 m. The location of maximum is found by varying the position of the center of the circle. By running different instruments design with several different geometries and adjustment of various reflector parameters (e.g. starting position, length, etc.) a large number of such optics can be investigated to find optimal parameters. In Fig. 8 the general sequence of a typical simulation cycle is shown.

The reflectivity R of the supermirror is calculated in McStas by applying an empirical formula derived from experimental data [28]:

$$R = \begin{cases} R_0 & \text{if } Q \le Q_c \\ \frac{1}{2} R_0 \left(1 - \tanh\left[\left(Q - mQ_c\right)/W\right]\right)\left(1 - \alpha\left(Q - Q_c\right)\right) & \text{if } Q > Q_c. \end{cases} \quad (3)$$

[1] https://mads-bertelsen.github.io/index.html.
[2] https://jupyter.org.

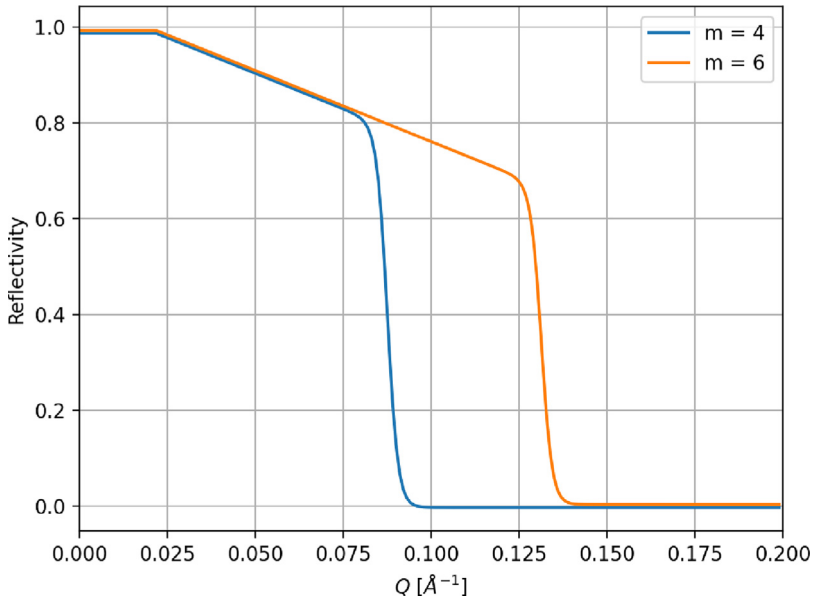

Fig. 10. Two typical reflectivity curves for a supermirror derived from Eq. (3).

Here R_0 is the low-angle reflectivity, Q_c is the critical scattering vector, α is the slope of reflectivity, W the width of the supermirror cut-off, and Q (in Å^{-1}) the length of the scattering vector of the incoming neutron. Non-specular reflection caused by e.g. surface roughness of the mirrors is currently not taken into account. The default settings of `McStas`, $R_0 = 0.99$, $Q_c = 0.0219\,\text{Å}^{-1}$, $\alpha = 3\,\text{Å}$ and $W = 0.003\,\text{Å}^{-1}$, resemble a typical supermirror and are sufficient to model the reflectors for the NNBAR simulations. In Fig. 10 two exemplary reflectivity curves for $m = 4$ and $m = 6$ are shown. The used components support currently only an overall reflectivity. So that the m value cannot vary across the optical component. The simulations for this work have been done using an m value of 6.

4.1. Construction of the nested optics

If the outer layer of a nested elliptical guide is given, the inner layers can be constructed in a recursive manner. A sketch of the construction is shown in Fig. 11 (y and z axis have been chosen in to comply with the coordinate system used in McStas). The source S and the detector D are located at the ellipses foci. b_n are the minor half-axes of the nth nested layers. The distance L between the two foci of the ellipse is related to the focal distance by the simple relation $f = L/2$. The following construction will be valid for start z_s and end z_e points that fulfill the criteria:

$$-f < z_s < z_e < f \tag{4}$$

From the sketch (Fig. 11) it is seen that a straight lines from the source position S to the end of the optics from an outer layer (index n) defines the starting position of the next layer (index $n + 1$). From this, an analytical expression for the minor half axes b_n of each layer can be calculated:

$$b_n = \sqrt{-\frac{\left(f^2 - z^2 - K_n^2\right)}{2} + \sqrt{\frac{(f^2 - z^2 - K_n^2)^2}{4} + K_n^2 f^2}}, \tag{5}$$

with

$$K_n = \frac{\tilde{z}_s}{\tilde{z}_e} y_{n-1}\left(z_e\right), \tag{6}$$

being obtained from the previous levels in recursive manner, where $\tilde{z}_s$ and $\tilde{z}_e$ are the distances from focal point S to the start resp. end of the optic (not to be confused with z_s (z_e) the coordinates of the starting (end) point of the optic). They are related by $\tilde{z}_s = z_s + f$ and $\tilde{z}_e = z_e + f$. Given the parameters of the outermost ellipse ($f = L/2$, b_0), the start and the end of the optics (z_s, z_e) all parameters are known to compute the small half-axis b_n of the inner layers of the nested optics. For all the nested optic variants of Fig. 5, functions to generate OFF-files have been developed. For a non-point like source, as is the LD2 moderator, the elliptic mirrors will lead to a smearing and possible screening effect of the nested layers (see Section 3.2). The method presented here to calculate the nested levels is not taking these effects into account. The size ratios of moderator and optical device justify this approach. Nevertheless they do have to be considered when analyzing and interpreting the simulations results.

5. Results

5.1. Baseline design and differential reflector

As a starting point for the simulations a so called "baseline" for comparison purposes was defined. It consists of an cylindrically shaped elliptical reflector of a single layer. It is further defined by the distance of 200 m between the two foci and a small semi axis b of 2 m. The center of the source (moderator) is located in one focus, while the center of the detector is located in the other focal point. The reflector covers the part of the ellipse that starts at 10 m from the source and ends at a distance of 50 m and is therefore 40 m long. Different sizes of the cold source moderator, the neutron emission spectra and the engineering constraints of the NNBAR-experiment can be studied for this standard baseline configuration. This baseline design scheme has, in addition, been previously used for optimization of parameters and for comparison of several NNBAR configurations in previous publications [2,13,31].

A `McStas` simulation performed with this reflector with the horizontal axis at the center of LBP gave a FOM = 333 with the moderator parameters and spectrum shown in the previous section for ESS power of 2 MW. The shape of the reflector and the focused beam distribution at the annihilation target obtained in the simulation are depicted in Fig. 12.

Since the center of lower moderator is ∼ 20 cm below the axis of the LBP (see Fig. 13), a reflector placed symmetrically relative to the moderator may not use the full aperture provided by the LBP.

To cope with that issue the concept of a "differential reflector" was proposed [31]. The reflector is positioned exactly in the middle of the LBP but has a distorted ellipsoid shape (See Fig. 13). The constituting

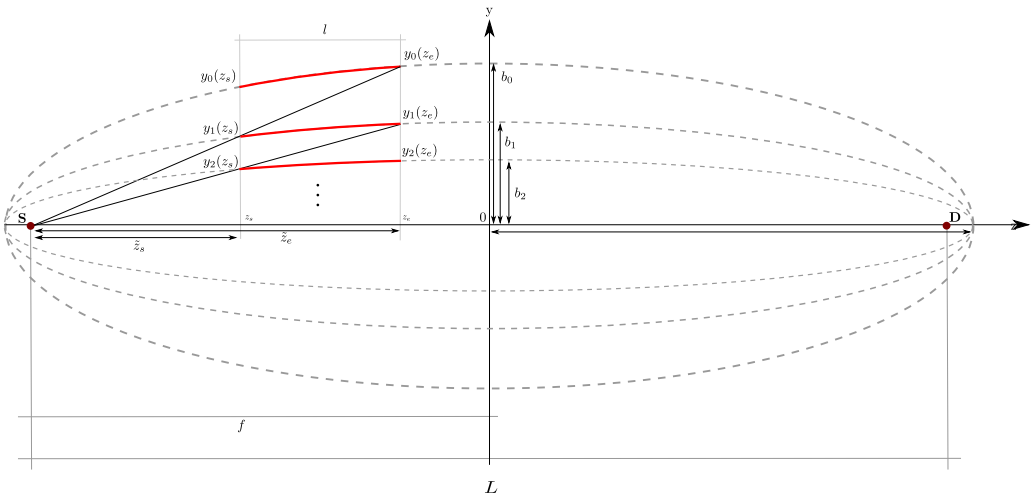

Fig. 11. Schematic of how the inner nested layers are constructed from the outer ones.

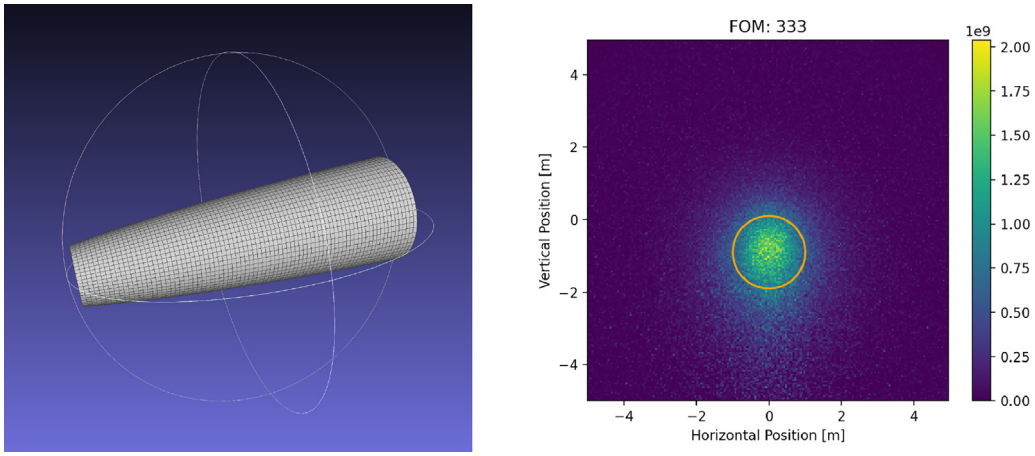

Fig. 12. (left) 3D Visualization of the 40 m long baseline reflector (axis are not in scale). (right) Result of a McStas simulation with the baseline reflector for Target Power 2 MW. The orange circle marks the detector area of 1 m radius. The FOM is 333.

Fig. 13. (left) Cross sectional view of the ESS target/moderator area and the inner shielding. In the figure it is shown the location of the ESS upper and lower moderator. The NNBAR experiment will view both moderators. (right) Depiction of the differential reflector.

panels fulfill the solution of a coupled differential equation, to behave on each position like an elliptical mirror and form a continuous surface. This reflector focuses and bends the neutron beam by a few degrees in the vertical direction at the same time. This will allow the preservation of the FOM with the horizontal beam axis between the centers of the cold source and the annihilation detector.

McStas simulations performed show the comparability of this layout to the baseline design. With the "differential reflector" a FOM = 340 is achieved, which amounts to a small increase of around 1% compared to the baseline.

5.2. Nested mirror layouts

The optimal parameters for the different possible geometries are studied by performing various simulations and comparing the obtained

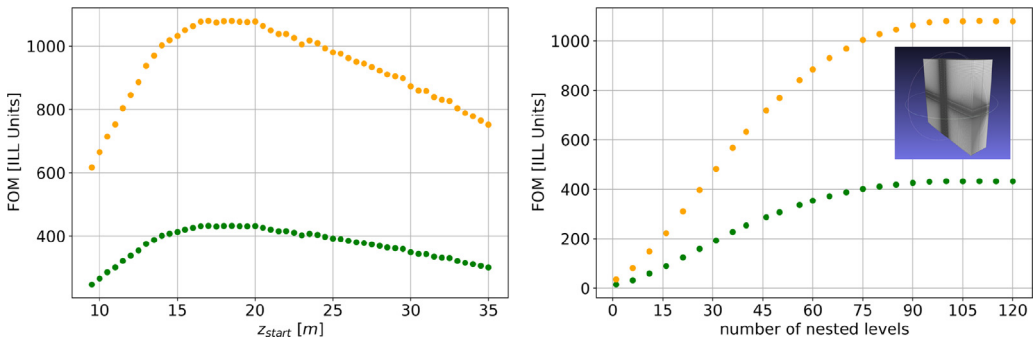

Fig. 14. Result of simulations for a nested double planar reflector of length 1 m (see inlay) for 2 MW (green) and 5 MW (orange) target power of the ESS. (left) Varying of the starting point of the optic. (right) Increasing the number of nested levels.

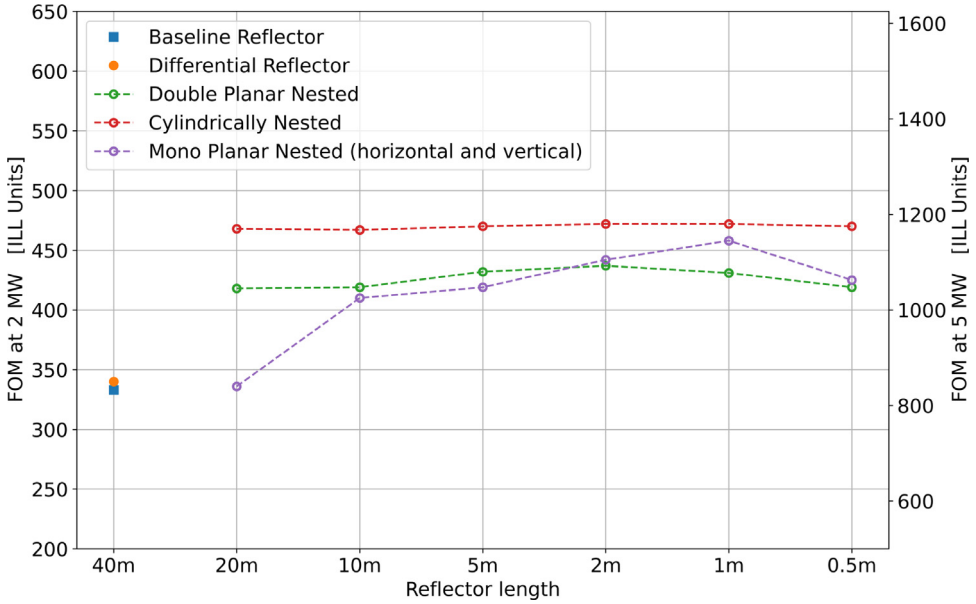

Fig. 15. Collected FOMs for different reflector geometries (target power 2 MW and 5 MW, respectively).

FOMs. Two such scans for a 1 m long double planar nested reflector are shown in Fig. 14. The scan for the z_{start} parameter (the start of the optic defined as distance from the moderator) shows an optimum at about 17 m. It should be noted that increasing the start-of-optics distance, say from 10 m to 20 m would increase the face size of the reflector by factor of 2. It demonstrates that the choice of the start-of-optics parameter should be made together with optimization of other parameters defining the sensitivity, including the overall cost. For the number of nested levels, one observes a saturation after a certain point, when adding further levels does not lead to a further increase of the FOM.

For the simulations of the mono planar components the one with mirrors in horizontal arrangement was always put in front of the one with mirrors in vertical layout. The reason has to do with the magnification. Since the moderator is in width 40 cm and in height 24 cm it is of advantage to have the vertical component with less magnification farther away from the moderator. The shorter the components get the less pronounced this effect becomes.

5.3. Collected results of the simulations

In the following Fig. 15 the results of the simulations for the various reflector geometries are summarized. With the nested components significantly higher FOMs than with the baseline or the differential reflector can be achieved. The cylindrical components slightly outperform the planar ones. This is due to the fact that the in the former only one reflection is necessary to each the target, while the later need an additional one. In general gains of at least 20% over the baseline reflector can be achieved.

The results of how the optimum starting locations z_{start} of the reflectors change is shown in Fig. 16. The shorter the reflector the about 17 m. With the length of the optics becoming shorter the optimal starting location is shifted farther away from the moderator.

6. Conclusion

This paper presents the results of a systematic study of different layouts of nested mirror optics for an NNBAR experiment. With these optics in simulations FOM $\geq$ 400 per year at 2 MW target power could be achieved. At this target power and a foreseen run time of the experiment of 2–3 years the goal of increasing the previous sensitivity by 3 orders of magnitude might be within reach. An upgraded target power of 5 MW would even let this goal to be reached in a running time of about 1 year. It has to be mentioned that the above would hold only in an ideal scenario. In future studies losses such as inaccuracies in assembling the components, surface roughness and the finite extension of the mirrors, have to be taken into account. This will lead to a reduction of the FOM and an increase in the running time of the experiment.

Both the reflector in its baseline configuration and the "differential reflector" will be large, mechanically complicated, logistically difficult to assemble and install, and therefore expensive. The "nested

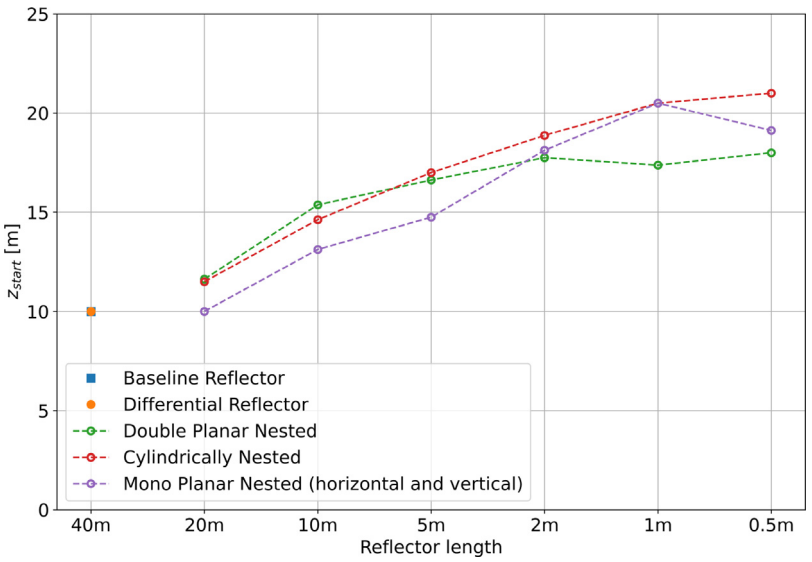

Fig. 16. Starting position z_{start} for the different reflector types and lengths. The optimum of shorter reflectors tends to be at positions further upstream.

reflectors" described in this paper seems to provide an even higher FOM, are more compact and can be much shorter in length along the beam axis. Although some difficulties in engineering them have to be overcome, too, they might be easier to construct and may represent a more economical solution for NNBAR. Most promising in this respect is the mono planar configuration that consists of two separated nested reflectors that act in horizontal resp. vertical direction. The sizes of the reflectors that can be attained in a realistic setup will be looked at in a next step as part of a Conceptual Design Report for the NNBAR experiment.

Measurements with small scale prototypes (optical lengths about 10 cm) of this kind of reflectors (see [32]) have been recently performed and showed the principal feasibility to actually build these type of nested reflectors. These results are promising. The large size of the reflector needed for NNBAR is still challenging, but a prototype of intermediate size might be a way forward. For such prototypes the efficiency of the neutron supermirror and especially the impact of non-specular reflection on the performance of such optics have to be studied as part of future experimental work.

Declaration of competing interest

The authors declare the following financial interests/personal relationships which may be considered as potential competing interests: R.Wagner reports financial support was provided by European Commission.

Data availability

Data will be made available on request.

Acknowledgments

This work was funded by the HighNESS project at the European Spallation Source. HighNESS is funded by the European Framework for Research and Innovation Horizon 2020, under grant agreement 951782. Support was also given by the Swedish Research Council, Vetenskapsrådet.

References

[1] A.D. Sakharov, Violation of CP Invariance, C asymmetry, and baryon asymmetry of the universe, Pis'ma Zh. Eksp. Teor. Fiz. 5 (1967) 32–35.
[2] D.G. Phillips II, et al., Neutron-antineutron oscillations: Theoretical status and experimental prospects, Phys. Rep. 612 (2016) 1–45.
[3] K.S. Babu, P.S. Bhupal Dev, E.C.F.S. Fortes, R.N. Mohapatra, Post-sphaleron baryogenesis and an upper limit on the neutron-antineutron oscillation time, Phys. Rev. D 87 (11) (2013) 115019.
[4] S. Patra, P. Pritimita, Post-sphaleron baryogenesis and n - $\bar{n}$ oscillation in non-SUSY SO(10) GUT with gauge coupling unification and proton decay, Eur. Phys. J. C 74 (10) (2014) 3078.
[5] P.-H. Gu, U. Sarkar, High-scale baryogenesis with testable neutron-antineutron oscillation and dark matter, Phys. Rev. D 96 (3) (2017) 031703.
[6] R. Barbier, et al., R-parity violating supersymmetry, Phys. Rep. 420 (2005) 1–202.
[7] L. Calibbi, G. Ferretti, D. Milstead, C. Petersson, R. Pöttgen, Baryon number violation in supersymmetry: n-nbar oscillations as a probe beyond the LHC, J. High Energy Phys. 05 (2016) 144, [Erratum: JHEP 10, 195 (2017)].
[8] P.T. Winslow, J.N. Ng, Neutron-antineutron oscillations in a warped extra dimension, Phys. Rev. D 81 (2010) 106010.
[9] S. Nussinov, R. Shrock, N - anti-N oscillations in models with large extra dimensions, Phys. Rev. Lett. 88 (2002) 171601.
[10] M. Baldo-Ceolin, et al., A New experimental limit on neutron - anti-neutron oscillations, Z. Phys. C 63 (1994) 409–416.
[11] A. Fomin, A. Serebrov, M. Chaikovskii, O. Zherebtsov, A. Murashkin, E. Golubeva, Plan of NNbar Experiment at the WWR-M Reactor, 219 (2019) 07003.
[12] V. Gudkov, E. Klinby, B. Meirose, D. Milstead, V.V. Nesvizhevsky, K.V. Protasov, N. Rizzi, V. Santoro, W.M. Snow, R. Wagner, S.-C. Yiu, A Possible Neutron-Antineutron Oscillation Experiment at PF1B at the Institut Laue Langevin, 13 (2021) 2314.
[13] A. Addazi, et al., New high-sensitivity searches for neutrons converting into antineutrons and/or sterile neutrons at the HIBEAM/NNBAR experiment at the European Spallation Source, J. Phys. G: Nucl. Part. Phys. 48 (7) (2021) 070501.
[14] S. Peggs, ESS technical design report, 2013.
[15] V. Santoro, et al., Development of a high intensity neutron source at the European spallation source: The highNESS project, in: 14th International Topical Meeting on Nuclear Applications of Accelerators, 2022, arXiv:2204.04051.
[16] V. Santoro, The HighNESS Project and Future Free Neutron Oscillations Searches at the ESS, PoS EPS-HEP2021, 2022, p. 711.
[17] S.-C. Yiu, et al., Status of the design of an annihilation detector to observe neutron-antineutron conversions at the European spallation source, Symmetry 14 (1) (2022) 76.
[18] F. Backman, J. Barrow, Y. Beßler, A. Bianchi, C. Bohm, G. Brooijmans, H. Calen, J. Cederkäll, J. Damian, E. Dian, D. Di Julio, K. Dunne, L. Eklund, M. Ferreira, P. Fierlinger, U. Friman-Gayer, C. Happe, M. Holl, T. Johansson, Y. Kamyshkov, E. Klinkby, R. Kolevatov, A. Kupsc, B. Meirose, D. Milstead, A. Nepomuceno, T. Nilsson, A. Oskarsson, H. Perrey, K. Ramic, B. Rataj, N. Rizzi, V. Santoro, S. Silverstein, W. Snow, A. Takibayev, R. Wagner, M. Wolke, S. Yiu, A. Young, L. Zanini, O. Zimmer, The Development of the NNBAR Experiment, 17 (2022) P10046.

[19] S.-C. Yiu, B. Meirose, J. Barrow, C. Bohm, G. Brooijmans, K. Dunne, E.S. Golubeva, D. Milstead, A. Nepomuceno, A. Oskarsson, V. Santoro, S. Silverstein, Status of the design of an annihilation detector to observe neutron-antineutron conversions at the European spallation source, Symmetry 14 (1) (2022).
[20] Supermirrors for Neutrons, Swiss Neutronics Co, 2021.
[21] Y. Kamyshkov, et al., Use of cold source and large reflector mirror guide for neutron-antineutron oscillation search, 1995, pp. 843–849.
[22] O. Zimmer, Multi-mirror imaging optics for low-loss transport of divergent neutron beams and tailored wavelength spectra, 2016, arXiv:1611.07353 [Hep-Ex, Physics:Nucl-Ex, Physics:Physics].
[23] O. Zimmer, Imaging nested-mirror assemblies – A new generation of neutron delivery systems? J. Neutron Res. 20 (4) (2019) 91–98.
[24] H. Shimizu, Optimization of supermirror, 2014, URL: https://indico.esss.lu.se/event/171/contributions/1335/attachments/1140/1796/20140612-shimizu.pdf.
[25] D.M. Rodriguez, S.J. Kennedy, P.M. Bentley, Properties of Elliptical Guides for Neutron Beam Transport and Applications for New Instrumentation Concepts, 44 (2011) 727–737.
[26] J. Barrow, et al., Computing and detector simulation framework for the HIBEAM/NNBAR experimental program at the ESS, EPJ Web Conf. 251 (2021) 02062.
[27] P. Willendrup, E. Farhi, K. Lefmann, McStas 1.7 - a new version of the flexible Monte Carlo neutron scattering package, Physica B 350 (1, Supplement) (2004) E735–E737, Proceedings of the Third European Conference on Neutron Scattering.
[28] P. Willendrup, E. Farhi, E. Knudsen, U. Filges, K. Lefmann, Component manual for the neutron ray-tracing package McStas, 2020, http://www.mcstas.org/documentation/manual/mcstas-2.7-components.pdf.
[29] T. Kittelmann, E. Klinkby, E. Knudsen, P. Willendrup, X. Cai, K. Kanaki, Monte Carlo particle lists: MCPL, Comput. Phys. Comm. 218 (2017) 17–42.
[30] J. Goorley, M. James, et al., Initial MCNP6 Release Overview, Technical Report LA-UR-13-22934, Los Alamos National Laboratory, 2013.
[31] M. Frost, Observation of Baryon Number Violation via Cold Neutron Sources (Ph.D. thesis), University of Tennessee, Knoxville, 2019, URL: https://trace.tennessee.edu/utk_graddiss/5951.
[32] C. Herb, O. Zimmer, R. Georgii, P. Böni, Nested mirror optics for neutron extraction, transport, and focusing, Nucl. Instrum. Methods Phys. Res. A 1040 (2022) 167154.